Analysis of the neutron noise induced by fuel assembly vibrations

Andrea Zoia[a,*], Amélie Rouchon[a], Baptiste Gasse[a], Christophe Demazière[b], Paolo Vinai[b]

[a] *Université Paris-Saclay, CEA, Service d'études des réacteurs et de mathématiques appliquées, 91191, Gif-sur-Yvette, France*
[b] *Chalmers University of Technology, Department of Physics, Division of Subatomic and Plasma Physics, SE-41296 Gothenburg, Sweden*

Abstract

The investigation of neutron noise is key to several applications in nuclear reactor physics, such as the detection of control rod or assembly vibrations and the diagnostic of coolant speed and void fraction. In this paper we will elucidate some aspects of the noise equations in the Fourier domain, for the case of periodic fuel rod vibrations with frequency ω_0 in a small symmetrical system in which the perturbation is centrally located. We will in particular focus on the double frequency effect, i.e., the emergence of a noise component at $2\omega_0$ (possibly stronger than the one at the fundamental frequency ω_0). Our analysis will be carried out without truncating the noise source at the first order and in the context of a non-perturbative approach (i.e., without resorting to linearization). For this purpose, we will select a simple benchmark configuration that is amenable to accurate reference solutions obtained by solving the exact time-dependent transport equations. The analysis carried out in this work suggests that the non-perturbative noise equations are mandatory in order to properly discriminate the possible emergence of double frequency effects in neutron noise, especially in view of comparing simulation results to experimental data.

Keywords: Neutron noise, Frequency domain, Linearized equations, Non-perturbative approach, Harmonics

*Corresponding author
Email address: andrea.zoia@cea.fr (Andrea Zoia)

1. Introduction

Power reactor noise is defined as the fluctuations of the neutron flux around the steady state, due to temperature or density changes and/or displacements of core components, which in turn induce fluctuations on the material cross sections (Pazsit and Demazière, 2010). Despite usually being an unwanted phenomenon, such fluctuations carry an information content that can be usefully extracted for the purpose of reactor diagnostics and measurements (Pazsit and Demazière, 2010; Williams, 1974; Thie, 1981). The analysis of the neutron flux variations at the local or global scale within the core can be used e.g. in order to detect anomalies (Behriguer et al., 1977; Fry et al., 1986), as in the case of control rod or assembly vibrations (Pazsit and Analytis, 1980), or infer the coolant speed and void fraction (Kosály, 1980).

Traditionally, the equations governing the neutron noise are derived based on a small-perturbation formulation: a perturbation of the Boltzmann operator is assumed to induce a response of the same order for the neutron flux, and the terms containing both the perturbed flux and the perturbed cross sections will be neglected by supposing that they will yield higher-order contributions (Pazsit and Demazière, 2010; Williams, 1974). This approach, dubbed the 'orthodox method' (Pazsit, 1984), allows obtaining simpler equations for the neutron noise, which are finally Fourier-transformed in order to establish the customary linearized noise equations in the frequency domain (Pazsit and Demazière, 2010; Williams, 1974). Such strategy has led to the development of ingenuous analytical tools, mostly relying on the use of Green's functions in diffusion theory, which have been successfully applied to the analysis of many practical diagnosis and monitoring problems (Pazsit and Analytis, 1980; Jonsson et al., 2012; Pazsit and Karlsson, 1996; Yamamoto and Sakamoto, 2019; Pazsit and Dykin, 2018); for a review, see, e.g., (Pazsit and Demazière, 2010; Williams, 1974). In the context of vibrating noise sources, a common approximation is to represent the spatial shape of the perturbation as an idealized delta function (the so-called Feinberg-Galanin-Williams model (Williams, 1970)), which might help in obtaining closed-form solutions for simple one-dimensional configurations.

The orthodox method is known to yield to correct results for the case of absorbers of variable strength (Williams, 1974; Thie, 1981; Kosály, 1980), but generally fails for the case of absorber or fuel rod vibrations (Pazsit, 1977): these considerations were implicit already in the seminal work of (Weinberg and Schweinler, 1948) and are discussed at length in (Pazsit, 1984). When the neutron noise is induced by vibrations, with a material region (e.g., a fuel rod or a control rod) moving in a host medium (e.g., the surrounding moderator), the am-

plitude of the cross section fluctuations cannot be assumed to be small, except under special conditions, such as in the limit case of weak absorbers (Weinberg and Schweinler, 1948; Pazsit, 1984). For the case of a vibrating absorber, the main reason for the failure of the linearized noise equations is that the neglected term contains a contribution of the same order as the perturbation, which can only be made small when the absorber strength is also small (Pazsit, 1984). Nonetheless, it has been shown that the orthodox method may still provide accurate estimates for the neutron noise when the vibration amplitude ε is small with respect to the typical size d of the vibrating body projected in the direction of the vibration, i.e., $\varepsilon/d \ll 1$ (Pazsit, 1984; Pazsit and Karlsson, 1996), as suggested by the boundary-perturbation theory (Rahnema, 1996; Sanchez, 2015). Similar conclusions for the case of vibration-induced neutron noise were more recently drawn in (Rouchon and Sanchez, 2015; Sanchez, 2015; Rouchon, 2016).

Furthermore, within the framework of the linearized equations combined with the ε/d approximation for vibration-induced noise, a common assumption consists in keeping only the leading-order term of the noise source, which corresponds to the contribution at the fundamental frequency ω_0 of the vibration: by virtue of the linearity of the noise equations, the system will thus respond only at ω_0 (Pazsit, 1977, 1984). This leads to the important issue of the 'double frequency' effect (Pazsit, 1977), i.e., ascertaining whether a system subject to a periodic vibration at frequency ω_0 can possibly exhibit a secondary spectral peak at $2\omega_0$ in the Fourier-transformed response, as suggested by some experiments (Lucia et al., 1973). This is in principle allowed when the noise source is treated exactly (Antonopoulos-Domis, 1976; Pazsit, 1977). For the case of weak absorbers, it has been shown that the amplitude of the secondary peak will be typically small (Pazsit, 1977). However, several works have hinted out that the emergence of a peak at $2\omega_0$ might be non-trivially related to the spatial shape of the flux gradients through the vibrating region, as shown by a careful treatment based on Green's functions in diffusion theory (Antonopoulos-Domis, 1976; Pazsit, 1977, 1984). Quite surprisingly, continuous-energy Monte Carlo simulations of the linearized noise equations independently performed by CEA and Kyoto University have also pointed out that in some circumstances the spectral peak at $2\omega_0$ might become (much) larger than the one at ω_0 [1].

Neutron noise analysis is nowadays mostly based on state-of-the-art numerical codes, capable of taking into account arbitrary cross section variations in the time or frequency domain (Demazière, 2011; Yamamoto, 2013; Rouchon et al., 2017; Rohde et al., 2018; Olmo-Juan et al., 2019; Vidal-Ferrándiz et al., 2020;

[1] T. Yamamoto, personal communication, 2019.

Chionis et al., 2020), as witnessed by the renewed interest stimulated by the CORTEX H2020 project (Demazière et al., 2018). For the case of frequency domain, newly developed transport (as opposed to diffusion) solvers (Rouchon, 2016; Yi et al., 2019) and Monte Carlo methods (Yamamoto, 2013; Rouchon et al., 2017) allow addressing realistic applications at the scale of fuel assemblies or full reactor cores with unprecedented accuracy (Demazière, 2011; Rouchon, 2016; Yamamoto, 2018; Mylonakis et al., 2019; Rouchon et al., 2019). However, one must bear in mind that each numerical tool has specific potentialities and drawbacks, as well as implicit assumptions due to the choices made by the code developers, such as working with the linearized equations, introducing the ε/d approximation, truncating the noise source, and so on. In this respect, the reliability of these codes inherently depends on a deeper understanding of the validity domain of the underlying models: the goal of the present work is to elucidate the behaviour of the noise equations, and in particular the double frequency effect, when the source is not truncated at the first order and in the context of a non-perturbative approach (i.e., without resorting to linearization). For this purpose, we will use a simple benchmark configuration, namely, a single vibrating fuel rod centrally located in a host moderator, which avoids unnecessary complications and yet retains the key physical ingredients.

This paper is organized as follows. In Sec. 2 we briefly recall the formalism of the neutron noise equations and the orthodox linearization. In Sec. 3 we introduce the noise source pertaining to the case of mechanical vibrations, and examine the contributions of the discrete harmonics of the source. In order to illustrate the behaviour of the noise field and the interplay of the different harmonics, in Sec. 4 we present a benchmark based on the rod model, a one-dimensional, single-speed neutron transport problem, and discuss our findings within the framework of the linearized noise theory. The solutions corresponding to the non-perturbative approach will be derived and contrasted to those of the linearized equations in Sec. 5. Conclusions will be finally drawn in Sec. 6.

2. The noise equation(s) and the orthodox linearization

Let us consider a nuclear system at equilibrium, whose balance equation for the critical neutron flux $\varphi_c(\mathbf{r}, \mathbf{\Omega}, E)$ reads $\mathcal{B}_c\varphi_c = 0$, where

$$\begin{aligned}\mathcal{B}_c = \mathbf{\Omega}\cdot\nabla + \Sigma_t - \int\int f_s(\mathbf{\Omega}'\cdot\mathbf{\Omega}, E' \to E)\Sigma_s(\mathbf{r}, E')dE'd\mathbf{\Omega}' \\ -\frac{\chi_p(E)}{4\pi k_{\text{eff}}}\int\int \nu_p(E')\Sigma_f(\mathbf{r}, E')dE'd\mathbf{\Omega}' \\ -\sum_j \frac{\chi_d^j(E)}{4\pi k_{\text{eff}}}\int\int \nu_d^j(E')\Sigma_f(\mathbf{r}, E')dE'd\mathbf{\Omega}' \end{aligned} \tag{1}$$

is the stationary Boltzmann operator, with associated fundamental eigenvalue $k_{\text{eff}} \simeq 1$, and the sum is extended over the precursor families. Notation is standard, and for the sake of simplicity we have assumed here that a single fissile isotope is present. Suppose now that a perturbation possibly involving material displacements is introduced in the system, with the perturbed cross sections $\Sigma_\alpha(t) = \Sigma_\alpha(\mathbf{r}, E, t)$ evolving in time according to a given law, α being the index of a specific reaction. Correspondingly, the perturbed neutron flux $\varphi(t) = \varphi(\mathbf{r}, \mathbf{\Omega}, E, t)$ will be ruled by the perturbed time-dependent Boltzmann equation $\mathcal{B}_p(t)\varphi(t) = 0$, where

$$\begin{aligned}\mathcal{B}_p(t) = \frac{1}{\upsilon}\frac{\partial}{\partial t} + \mathbf{\Omega}\cdot\nabla + \Sigma_t(\mathbf{r}, E, t) \\ -\int\int f_s(\mathbf{\Omega}'\cdot\mathbf{\Omega}, E' \to E)\Sigma_s(\mathbf{r}, E', t)dE'd\mathbf{\Omega}' \\ -\frac{\chi_p(E)}{4\pi k_{\text{eff}}}\int\int \nu_p(E')\Sigma_f(\mathbf{r}, E', t)dE'd\mathbf{\Omega}' \\ -\sum_j \lambda_j\frac{\chi_d^j(E)}{4\pi k_{\text{eff}}}\int\int\int e^{-\lambda_j(t-t')}\nu_d^j(E')\Sigma_f(\mathbf{r}, E', t')dE'd\mathbf{\Omega}'dt' \end{aligned} \tag{2}$$

is the time-dependent Boltzmann operator, including the contributions of the delayed neutron precursors.

The perturbation is supposed to have started at some previous time, sufficiently far in the past for the system to have reached its asymptotic behaviour at time $t = 0$ (the initial observation time). We will assume that the cross section

perturbations can be expressed as

$$\Sigma_\alpha(\mathbf{r},E,t) = \Sigma_\alpha(\mathbf{r},E) + \delta\Sigma_\alpha(\mathbf{r},E,t), \tag{3}$$

where $\Sigma_\alpha(\mathbf{r},E)$ is the stationary part and $\delta\Sigma_\alpha(\mathbf{r},E,t)$ is the time-varying component. Correspondingly, we define the neutron noise $\delta\varphi(\mathbf{r},\mathbf{\Omega},E,t)$ as the time-varying part of the neutron field, and we decompose

$$\varphi(\mathbf{r},\mathbf{\Omega},E,t) = \varphi_c(\mathbf{r},\mathbf{\Omega},E) + \delta\varphi(\mathbf{r},\mathbf{\Omega},E,t). \tag{4}$$

We are thus led to the formulation of the noise equation

$$[\mathcal{B}(t) + \delta\mathcal{B}(t)]\,\delta\varphi(t) = -\delta\mathcal{B}(t)\varphi_c, \tag{5}$$

where we have introduced the reference Boltzmann operator

$$\begin{aligned}\mathcal{B}(t) = {} & \frac{1}{\upsilon}\frac{\partial}{\partial t} + \mathbf{\Omega}\cdot\nabla + \Sigma_t(\mathbf{r},E) \\ & - \int\int f_s(\mathbf{\Omega}'\cdot\mathbf{\Omega}, E' \to E)\Sigma_s(\mathbf{r},E')dE'd\mathbf{\Omega}' \\ & - \frac{\chi_p(E)}{4\pi k_{\text{eff}}}\int\int \nu_p(E')\Sigma_f(\mathbf{r},E')dE'd\mathbf{\Omega}' \\ & - \sum_j \lambda_j \frac{\chi_d^j(E)}{4\pi k_{\text{eff}}}\int\int\int e^{-\lambda_j(t-t')}\nu_d^j(E')\Sigma_f(\mathbf{r},E')dE'd\mathbf{\Omega}'dt'\end{aligned} \tag{6}$$

and the perturbation of the Boltzmann operator

$$\begin{aligned}\delta\mathcal{B}(t) = {} & \delta\Sigma_t(\mathbf{r},E,t) - \int\int f_s(\mathbf{\Omega}'\cdot\mathbf{\Omega}, E' \to E)\delta\Sigma_s(\mathbf{r},E',t)dE'd\mathbf{\Omega}' \\ & - \frac{\chi_p(E)}{4\pi k_{\text{eff}}}\int\int \nu_p(E')\delta\Sigma_f(\mathbf{r},E',t)dE'd\mathbf{\Omega}' \\ & - \sum_j \lambda_j \frac{\chi_d^j(E)}{4\pi k_{\text{eff}}}\int\int\int e^{-\lambda_j(t-t')}\nu_d^j(E')\delta\Sigma_f(\mathbf{r},E',t')dE'd\mathbf{\Omega}'dt'.\end{aligned} \tag{7}$$

Equation (5) corresponds to formally decomposing the perturbed Boltzmann operator as $\mathcal{B}_p(t) = \mathcal{B}(t) + \delta\mathcal{B}(t)$. The term on the right-hand side of Eq. (5) represents the noise source, depending on the stationary flux φ_c (Pazsit and Demazière, 2010; Williams, 1974). No approximations have been introduced so

far.

2.1. Fourier analysis and linearization

The analysis of the noise equations is often carried out in the frequency domain. By applying the Fourier transform

$$f(\omega) = \mathcal{F}\left[f(t)\right](\omega) = \int_{-\infty}^{+\infty} e^{-i\omega t} f(t) dt \tag{8}$$

and using the convolution theorem

$$\mathcal{F}\left[f(t)g(t)\right](\omega) = \frac{1}{2\pi}\mathcal{F}\left[f(t)\right](\omega) \star \mathcal{F}\left[g(t)\right](\omega) = \frac{1}{2\pi}\int d\omega' f(\omega-\omega')g(\omega'), \tag{9}$$

where $\star$ denotes the convolution product, Eq. (5) yields the Fourier-transformed exact noise equation

$$\mathcal{B}(\omega)\delta\varphi(\omega) + \frac{1}{2\pi}\int \delta\mathcal{B}(\omega-\omega')\delta\varphi(\omega')d\omega' = -\delta\mathcal{B}(\omega)\varphi_c \tag{10}$$

in the frequency domain (Sanchez, 2015; Rouchon and Sanchez, 2015; Rouchon, 2016). Here we have introduced the Fourier-domain reference Boltzmann operator

$$\begin{aligned}\mathcal{B}(\omega) = {} & i\frac{\omega}{v} + \Sigma_t(\mathbf{r},E) + \mathbf{\Omega}\cdot\nabla - \int\int f_s(\mathbf{\Omega}'\cdot\mathbf{\Omega}, E' \to E)\Sigma_s(\mathbf{r},E')dE'd\mathbf{\Omega}' \\ & - \frac{\chi_p(E)}{4\pi k_{\text{eff}}}\int\int \nu_p(E')\Sigma_f(\mathbf{r},E')dE'd\mathbf{\Omega}' \\ & - \sum_j \frac{\lambda_j}{\lambda_j+i\omega}\frac{\chi_d^j(E)}{4\pi k_{\text{eff}}}\int\int \nu_d^j(E')\Sigma_f(\mathbf{r},E')dE'd\mathbf{\Omega}'\end{aligned} \tag{11}$$

and the Fourier-domain perturbation operator

$$\begin{aligned}\delta\mathcal{B}(\omega) = {} & \delta\Sigma_t(\mathbf{r},E,\omega) - \int\int f_s(\mathbf{\Omega}'\cdot\mathbf{\Omega}, E' \to E)\delta\Sigma_s(\mathbf{r},E',\omega)dE'd\mathbf{\Omega}' \\ & - \frac{\chi_p(E)}{4\pi k_{\text{eff}}}\int\int \nu_p(E')\delta\Sigma_f(\mathbf{r},E',\omega)dE'd\mathbf{\Omega}' \\ & - \sum_j \frac{\lambda_j}{\lambda_j+i\omega}\frac{\chi_d^j(E)}{4\pi k_{\text{eff}}}\int\int \nu_d^j(E')\delta\Sigma_f(\mathbf{r},E',\omega)dE'd\mathbf{\Omega}'.\end{aligned} \tag{12}$$

Equation (10) is a Boltzmann-like transport equation for the complex neutron noise field $\delta\varphi(\omega)$, where the operators $\mathcal{B}(\omega)$ and $\delta\mathcal{B}(\omega)$ as well as the source term $-\delta\mathcal{B}(\omega)\varphi_c$ are complex.

The *orthodox* approach to the noise theory consists in neglecting the terms of the form $\delta\Sigma_\alpha(t)\delta\varphi(t)$ appearing in $\delta\mathcal{B}(t)\delta\varphi(t)$ in Eq. (5), based on the assumption that the product of the two perturbed terms is small as compared to the perturbation of each term in the product (Pazsit, 1984). Under this hypothesis, we can drop the convolution product from Eq. (10), which yields the customary formulation of the *linearized noise equation* in the frequency domain, namely

$$\mathcal{B}(\omega)\delta\varphi(\omega) = -\delta\mathcal{B}(\omega)\varphi_c. \tag{13}$$

By opposition, we will call Eq. (10) the *non-perturbative* formulation of the Fourier-transformed noise equations.

3. The source term: the case of interface vibrations

The source term $-\delta\mathcal{B}(\omega)\varphi_c$ appears both in Eq. (10) and in Eq. (13) and does not depend on whether we consider the exact or linearized noise equations. However, the source term does depend on the specific assumptions on the noise model for the system under consideration: the operator $\delta\mathcal{B}(\omega)$ contains terms of the kind $\delta\Sigma_\alpha(\mathbf{r}, E, \omega)$, expressing the Fourier-transformed cross section perturbation for a given reaction α.

In the following, we will assume that the neutron noise is induced by one or several vibrating interfaces between homogeneous materials. Let us focus on the case where the vibration acts along a single axis, say x, and let us denote by x_0 the unperturbed position of the interface [2]. We define $\Sigma_\alpha^L(E)$ and $\Sigma_\alpha^R(E)$ the spatially homogeneous cross sections of the regions at the left ($x < x_0$) and the right ($x > x_0$), respectively, of the interface at x_0. We assume that the vibration is *periodic*, with frequency ω_0 and period $T_0 = 2\pi/\omega_0$, and with amplitude ε smaller than the linear size d of the region concerned by the interface perturbation. The position of the moving interface will be described by $x_i(t) = x_0 + \varepsilon\sin(\omega_0 t)$, with $x_0 - \varepsilon < x_i(t) < x_0 + \varepsilon$.

Under these assumptions, the general form of the interface perturbation in

[2] The generalization to the case where the vibration has several components along the three Cartesian axes can be carried out by following the same arguments, at the expense of more cumbersome calculations.

the time domain is

$$\delta\Sigma_\alpha(x,E,t) = \Delta\Sigma_\alpha(E)\,[H(x-x_0) - H(x-x_0-\varepsilon\sin(\omega_0 t))]\,, \tag{14}$$

where $\Delta\Sigma_\alpha(E) = \Sigma_\alpha^L(E) - \Sigma_\alpha^R(E)$ and $H(z)$ is the Heaviside function, with $H(z) = 1$ for $z \geq 0$, and $H(z) = 0$ otherwise. Observe that $\delta\Sigma_\alpha(x,E,t)$ is non-zero only in the region traversed by the vibrating interface, namely, $x_0 - \varepsilon \leq x \leq x_0 + \varepsilon$.

3.1. The ε/d approximation

Before investigating the behaviour of the exact source term in Eq. (14), it is instructive to consider the ε/d approximation (Pazsit, 1977). When the amplitude ε of the perturbation is small as compared to d, Eq. (14) can be expanded in powers of ε, by using the Taylor series

$$H(z+\varepsilon) = H(z) + \varepsilon\delta(z) + \frac{\varepsilon^2}{2}\delta'(z) + \cdots\,, \tag{15}$$

$\delta(z)$ and $\delta'(z)$ being the delta distribution and its derivative, respectively. We therefore have

$$\delta\Sigma_\alpha(x,E,t) = \Delta\Sigma_\alpha(E)\left[\varepsilon\sin(\omega_0 t)\delta(x-x_0) - \frac{\varepsilon^2\sin^2(\omega_0 t)}{2}\delta'(x-x_0) + \cdots\right], \tag{16}$$

whose effect is spatially localized at the stationary position x_0 of the interface. Now, by using

$$\mathcal{F}[\sin(\omega_0 t)] = -i\pi\,[\delta(\omega-\omega_0) - \delta(\omega+\omega_0)] \tag{17}$$

and

$$\mathcal{F}[\sin^2(\omega_0 t)] = \pi\delta(\omega) - \frac{\pi}{2}\,[\delta(\omega-2\omega_0) + \delta(\omega+2\omega_0)] \tag{18}$$

we obtain the Fourier-transformed expansion

$$\begin{aligned}\delta\Sigma_\alpha(x,E,\omega) =& \Delta\Sigma_\alpha(E)[-i\pi\varepsilon\delta(x-x_0)\delta(\omega-\omega_0) \\ &+ \frac{\pi}{4}\varepsilon^2\delta'(x-x_0)\delta(\omega-2\omega_0) + \cdots],\end{aligned} \tag{19}$$

where we have neglected the contributions associated to $\omega = 0$ and to negative frequencies, for reasons that will be discussed later. In the Fourier domain, the effect of an interface periodically vibrating at a frequency ω_0 is thus mirrored in an infinite sum of contributions corresponding to discrete frequencies, each

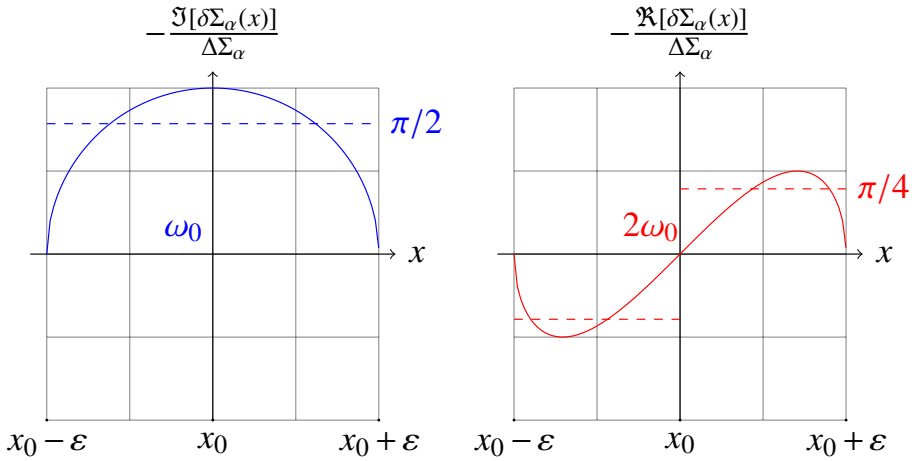

Figure 1: The spatial shape of the noise source. Comparison between the ε/d approximation (plotted as a dashed line, using the nascent functions to represent the singular spatial behaviour located at the interface) and the exact representation (plotted as solid line). Left: the imaginary part of the component at ω_0; right: the real part of the component at $2\omega_0$.

multiple of the fundamental frequency ω_0 of the forcing function and with decreasing amplitudes.

Although many authors have pointed out that the second harmonic might in some cases be relevant (Lucia et al., 1973; Antonopoulos-Domis, 1976; Pazsit, 1977, 1984), the Taylor expansion in Eq. (19) has been truncated at the first order in most of the previous works concerning neutron noise, thus including the contribution of the first harmonic alone. In view of the functional form of Eq. (19), one might suppose that the contribution of the second harmonic at $2\omega_0$ is ε times smaller than that of the first harmonic at ω_0. However, expression (19) is composed of a series of increasingly singular spatial functions localized at the interface position x_0. A common approximation consists in smoothing these contributions over the spatial region of the vibration, which is expedient for a numerical treatment (Vidal-Ferrándiz et al., 2020). For small ε, the delta distribution can be approximated by a suitable nascent delta function $F_\varepsilon(x)$ of the kind

$$\delta(x) \simeq F_\varepsilon(x) = \frac{1}{\varepsilon} F\left(\frac{x}{\varepsilon}\right), \tag{20}$$

with $F(z)$ being normalized [3] with respect to z. A widely adopted choice is to

[3] By a change of variables, it follows that $F_\varepsilon(x)$ is also normalized with respect to x.

assume

$$F_\varepsilon(x) = \frac{1}{2\varepsilon}|_{x\in[-\varepsilon,\varepsilon]}, \tag{21}$$

so that the ε term at the denominator cancels out with the prefactor of the first-order contribution in the Taylor expansion. As for the derivative of the delta distribution in the expansion given in Eq. (19), a convenient choice is the hat function

$$G_\varepsilon(x) = \frac{1}{\varepsilon}\left(1 - \frac{x}{\varepsilon}\mathrm{sign}\left(\frac{x}{\varepsilon}\right)\right)|_{x\in[-\varepsilon,\varepsilon]}. \tag{22}$$

We therefore have

$$\delta'(x) \simeq \frac{\partial}{\partial x}G_\varepsilon(x) = -\frac{1}{\varepsilon^2}\mathrm{sign}\left(\frac{x}{\varepsilon}\right)|_{x\in[-\varepsilon,\varepsilon]}, \tag{23}$$

so that ε^2 term at the denominator cancels out with the prefactor of the second-order contribution in the Taylor expansion.

Within the limits of the use of nascent functions to describe the singular spatial behaviour of the ε/d approximation, the first harmonic ω_0 will be thus associated to a negative imaginary contribution of amplitude $\pi/2$, spatially flat over the vibrating region, whereas the second harmonic $2\omega_0$ will be associated to a negative real contribution of amplitude $\pi/4$ (i.e., only half of the previous), spatially flat over the vibrating region on each side of the interface but changing sign across x_0 (see Fig. 1 for an illustration). These findings suggest that the effects of the second harmonic cannot be neglected a priori: under certain circumstances, basically depending on the spatial shape of the fundamental flux φ_c within the vibrating region [4], there might be a subtle competition between the Fourier component at ω_0 and the one at $2\omega_0$.

3.2. Analysis of the exact noise source

Bearing in mind the behaviour of the ε/d approximation, we can now examine the exact noise source for a periodically vibrating interface. Let us first consider the region $x > x_0$, where

$$\begin{aligned}\delta\Sigma_\alpha^R(x,E,t) =& \Delta\Sigma_\alpha(E)\left[1 - H(x - x_0 - \varepsilon\sin(\omega_0 t))\right] = \\ & \Delta\Sigma_\alpha(E)H(\varepsilon\sin(\omega_0 t) - x + x_0).\end{aligned} \tag{24}$$

[4] Recall that the expression of the noise source is $-\delta\mathcal{B}(\omega)\varphi_c$.

In this case, the Heaviside function is equal to unity when

$$\sin(\omega_0 t) \geq \frac{x - x_0}{\varepsilon}, \tag{25}$$

and zero otherwise, i.e., between time

$$\tau(x, x_0) = \frac{1}{\omega_0} \arcsin\left(\frac{x - x_0}{\varepsilon}\right) \tag{26}$$

and $T_0/2 - \tau(x, x_0) = \pi/\omega_0 - \tau(x, x_0)$. This condition yields a rectangular wave (Rouchon, 2016)

$$\delta\Sigma_\alpha^R(x, E, t) = \Delta\Sigma_\alpha(E)\left[\frac{1}{2} - \frac{\omega_0\tau(x, x_0)}{\pi} + 2\sum_{n=1}^{\infty} \frac{\sin\left(\frac{n\pi}{2} - n\omega_0\tau(x, x_0)\right)}{n\pi} \cos\left(\frac{n\pi}{2} - n\omega_0 t\right)\right], \tag{27}$$

whose Fourier transform yields

$$\delta\Sigma_\alpha^R(x, E, \omega) = \Delta\Sigma_\alpha(E)\left\{c_0^R(x, x_0)\delta(\omega) + \sum_{n=1}^{\infty} c_n^R(x, x_0)\left[\delta(\omega - n\omega_0) + \delta(\omega + n\omega_0)e^{in\pi}\right]\right\}. \tag{28}$$

Equation (28) defines an infinite sum of contributions corresponding to discrete frequencies $\pm n\omega_0$, $n = 0, 1, \cdots$, multiple of the fundamental frequency ω_0, in analogy with the findings for the ε/d approximation. The space-dependent Fourier coefficients appearing in Eq. (28) are given by

$$c_0^R(x, x_0) = \pi - 2\omega_0\tau(x, x_0) = \pi - 2\arcsin\left(\frac{x - x_0}{\varepsilon}\right) \tag{29}$$

and

$$c_n^R(x, x_0) = 2\frac{\sin\left(\frac{n\pi}{2} - n\omega_0\tau(x, x_0)\right)}{n} e^{-in\frac{\pi}{2}} = 2\frac{\sin\left(n\arccos\left(\frac{x - x_0}{\varepsilon}\right)\right)}{n} e^{-in\frac{\pi}{2}} \tag{30}$$

for $n \geq 1$, whose amplitude decreases with increasing n. In particular, the coefficient corresponding to the first harmonic at ω_0 is negative and imaginary:

$$c_1^R(x, x_0) = -2i\sqrt{1 - \left(\frac{x - x_0}{\varepsilon}\right)^2}; \tag{31}$$

for the second harmonic at $2\omega_0$ the coefficient is negative and real:

$$c_2^R(x, x_0) = -2\left(\frac{x - x_0}{\varepsilon}\right)\sqrt{1 - \left(\frac{x - x_0}{\varepsilon}\right)^2}. \tag{32}$$

More generally, all odd coefficients are imaginary, and all even coefficients are real. The spatially-averaged contributions are given by $\bar{c}_0^R = 2$,

$$\bar{c}_1^R = -\frac{\pi}{2}i, \tag{33}$$

and

$$\bar{c}_n^R = \frac{1}{\varepsilon}\int_{x_0}^{x_0+\varepsilon} c_n^R(x, x_0)dx = \frac{1 + e^{-i\pi n}}{1 - n^2} \tag{34}$$

for $n \geq 2$. This yields in particular

$$\bar{c}_2^R = -\frac{2}{3}. \tag{35}$$

The amplitude of the source term corresponding to the second harmonic is about twice as small as the one of the first harmonic, which is again consistent with the ε/d approximation. Observe that $\bar{c}_1^R$ is the only non-vanishing spatially-averaged coefficient for odd n.

For the region $x < x_0$, we have

$$\delta\Sigma_\alpha^L(x, E, t) = -\Delta\Sigma_\alpha(E)H(x - x_0 - \varepsilon\sin(\omega_0 t)). \tag{36}$$

In this case, the Heaviside function is equal to unity when

$$\sin(\omega_0 t) \leq \frac{x - x_0}{\varepsilon}, \tag{37}$$

and zero otherwise, i.e., between time $T_0/2 + \tau(x, x_0)$ and $T_0 - \tau(x, x_0)$. This condition defines a rectangular wave that is shifted by $T_0/2$ with respect to the one for the region $x > x_0$. By applying the Fourier transform, we have thus

$$\delta\Sigma_\alpha^L(x, E, \omega) = \\ \Delta\Sigma_\alpha(E)\left\{c_0^L(x, x_0)\delta(\omega) + \sum_{n=1}^{\infty} c_n^L(x, x_0)\left[\delta(\omega - n\omega_0) + \delta(\omega + n\omega_0)e^{in\pi}\right]\right\}, \tag{38}$$

where $c_n^L(x, x_0) = c_n^R(x, x_0)$ for $n \geq 1$, and $c_0^L(x, x_0) = c_0^R(x, x_0) - 2\pi$. The spatially-

averaged contributions are given by

$$\bar{c}_n^L = \frac{1}{\varepsilon}\int_{x_0-\varepsilon}^{x_0} c_n^L(x,x_0)dx, \tag{39}$$

which yields $\bar{c}_0^L = -\bar{c}_0^R$, $\bar{c}_1^L = \bar{c}_1^R$, $\bar{c}_n^L = 0$ for odd $n > 1$, and $\bar{c}_n^L = -\bar{c}_n^R$ for even $n \geq 2$. The spatial behaviour of the exact noise source is illustrated in Fig. 1.

3.3. Multiple interfaces

So far we have examined the effects of a single vibrating interface. The case of a region of size d vibrating into a host material can be dealt with by considering the linear superposition of the effects of two vibrating interfaces, each located at the boundaries of the region [5]. In this case, the terms $\Delta\Sigma_\alpha(E)$ corresponding to the respective boundaries will have opposite signs, so that one might possibly expect interference phenomena due to the simultaneous presence of two vibrating interfaces. The intensity of the interference of the interfaces will depend on the interplay between the vibration amplitude ε and the linear separation d between the boundaries: these effects will be discussed in Sec. 4, with the help of a numerical example.

3.4. Impact of the source on the noise field

Equations (28) and (38) completely define the Fourier spectrum of the noise source corresponding to a vibrating boundary between two homogeneous regions, for a sinusoidal displacement at a single frequency ω_0. The system will in principle respond to the vibration at several discrete frequencies $n\omega_0$, despite the impulsion being monochromatic at ω_0. The noise response

$$\mathcal{D}(\omega) = \int_D h_D(\mathbf{r},\mathbf{\Omega},E)\delta\varphi(\mathbf{r},\mathbf{\Omega},E,\omega)d\mathbf{r}d\mathbf{\Omega}dE \tag{40}$$

for a given frequency $\omega = n\omega_0$ will depend on the source intensity (i.e., on the Fourier coefficients $c_n^{R,L}(x,x_0)$ and on the shape of the fundamental flux φ_c), and on the noise detector function $h_D(\mathbf{r},\mathbf{\Omega},E)$, where the integral is defined over a region D of the phase space variables $\mathbf{r},\mathbf{\Omega},E$. The noise source term can be generally written as

$$-\delta\mathcal{B}(\omega)\varphi_c = -\sum_n \delta\mathcal{B}_n\varphi_c\delta(\omega - n\omega_0), \tag{41}$$

[5] Here we will assume that $\varepsilon < d/2$; the general case of arbitrary ε and d is discussed in (Rouchon, 2016).

with the appropriate noise source components $\delta\mathcal{B}_n$ associated to the cross section perturbations $\delta\Sigma_\alpha(\omega)$, to be inferred from Eqs. (28) and (38). We thus expect the noise field to be of the form (Sanchez, 2015; Rouchon, 2016)

$$\delta\varphi(\mathbf{r},\mathbf{\Omega},E,\omega)=\sum_n \delta\varphi_n(\mathbf{r},\mathbf{\Omega},E)\delta(\omega-n\omega_0), \tag{42}$$

where $\delta\varphi_n(\mathbf{r},\mathbf{\Omega},E)$ is the solution of the exact Fourier-transformed noise equation (10) corresponding to the noise source component at frequency $n\omega_0$, namely

$$\mathcal{B}_n\delta\varphi_n+\frac{1}{2\pi}\sum_m \delta\mathcal{B}_{n-m}\delta\varphi_m=-\delta\mathcal{B}_n\varphi_c. \tag{43}$$

Here we have denoted $\mathcal{B}_k=\mathcal{B}(k\omega_0)$ and $\delta\mathcal{B}_k=\delta\mathcal{B}(k\omega_0)$ the noise operator and the perturbation operator, respectively, evaluated at the discrete frequencies $k\omega_0$ of the source. This yields an infinite system of coupled equations for the noise components $\delta\varphi_n$, where the noise field at a given discrete frequency $n\omega_0$ depends on the behaviour of the noise field for all the other frequencies $m\omega_0$. For the orthodox approximation, Eq. (43) reduces to

$$\mathcal{B}_n\delta\varphi_n=-\delta\mathcal{B}_n\varphi_c, \tag{44}$$

which is an infinite system of fully decoupled linear equations [6] for the noise components $\delta\varphi_n$.

The noise source contributions due to negative frequencies $n<0$ can be dealt with by observing that $\delta\varphi_{-n}=\delta\varphi_n^\dagger$, where $\dagger$ denotes complex conjugation. Finally, the noise source contribution $-\mathcal{B}_0\varphi_c$, which involves the coefficients $c_0^{R,L}(x,x_0)$ and therefore corresponds to $\omega=0$ (i.e., the time-average of the perturbation), physically represents the offset due to the fact that the perturbation will in general introduce a non-vanishing reactivity effect in the system. For the linearized equations (13) all the components are decoupled from each other, so that the equation for $n=0$ will not influence the others and can be disregarded when solving for $n\geq 1$ (Sanchez, 2015; Rouchon, 2016). The effect of $-\mathcal{B}_0\varphi_c$ on the non-perturbative Eqs. (43) is more involved and the discussion of this case is deferred to Section 5.

[6] As a consequence, the n-th harmonic of the noise field only depends on the n-th order term of the noise source.

4. Analysis of the linearized noise equations: a benchmark model

In order to assess the linearized equations (13) combined with the exact model of the noise source (Eqs. (28) and (38)) or with the ε/d approximation (Eq. (19)), we consider the case of neutron noise due to vibrating interfaces in a benchmark configuration based on the *rod model*, which is possibly the simplest example of space- and direction-dependent transport problem (Wing, 1962; Montagnini and Pierpaoli, 1971): particles move at constant speed υ along a line (the rod) and undergo collision events with total cross section $\Sigma_t(x)$. Only two directions of flight are allowed, namely forward ($\mathbf{\Omega} = +$) and backward ($\mathbf{\Omega} = -$); we furthermore assume that the angular distributions for scattering and fission are isotropic. For the sake of simplicity, we will consider a single precursor family.

If we define $\delta\varphi^+(x)$ and $\delta\varphi^-(x)$ to be the (angular) neutron noise at position x in the positive and negative direction, respectively, the linearized noise equation (13) takes the form of two coupled ordinary first-order differential equations

$$\begin{aligned}&\left[i\frac{\omega}{\upsilon} \pm \frac{\partial}{\partial x} + \Sigma_t(x)\right]\delta\varphi^{\pm}(x,\omega)\\ &-\frac{1}{2}\left[\Sigma_s(x) + \frac{\nu_p\Sigma_f(x)}{k_{\text{eff}}} + \frac{\lambda}{\lambda+i\omega}\frac{\nu_d\Sigma_f(x)}{k_{\text{eff}}}\right]\delta\varphi(x,\omega) = Q^{\pm}(x,\omega),\end{aligned} \tag{45}$$

where $\delta\varphi(x) = \delta\varphi^+(x) + \delta\varphi^-(x)$ is the scalar noise integrated over the directions. We will assume that the viable space is a segment $[0, L]$, for some positive length L, with leakage boundary conditions $\delta\varphi^+(0,\omega) = 0$ and $\delta\varphi^-(L,\omega) = 0$. In principle, the Green's function of Eq. (45) could be determined exactly, by slightly adapting the analytical methods proposed in (Hoogenboom, 2008), and the solution would then follow by quadrature formulas with respect to the noise source term $Q^{\pm}(x,\omega)$. In practice, the resulting expressions are rather cumbersome, so that a numerical solution by discretization and matrix inversion has been chosen for this work. The noise source $Q^{\pm}(x,\omega) = -\delta\mathcal{B}(\omega)\varphi_c$ is given by

$$\begin{aligned}&Q^{\pm}(x,\omega) = -\delta\Sigma_t(x,\omega)\varphi_c^{\pm}(x)\\ &+\frac{1}{2}\left[\delta\Sigma_s(x,\omega) + \frac{\nu_p\delta\Sigma_f(x,\omega)}{k_{\text{eff}}} + \frac{\lambda}{\lambda+i\omega}\frac{\nu_d\delta\Sigma_f(x,\omega)}{k_{\text{eff}}}\right]\varphi_c(x),\end{aligned} \tag{46}$$

where $\varphi_c^{\pm}(x)$ is the fundamental mode corresponding to the stationary system, with associated eigenvalue k_{eff}, and $\varphi_c(x) = \varphi_c^+(x) + \varphi_c^-(x)$. The quantity $\delta\Sigma_\alpha(x,\omega)$ is the Fourier-transformed, spatially dependent cross section perturbation for re-

Figure 2: The rod model: a segment $[0, L]$ with three spatial regions separated by two interfaces at x_l and x_r.

action α, whose functional form for a vibrating interface is given in Eqs. (28) and (38).

The noise field $\delta\varphi^{\pm}(x,\omega)$ will be decomposed as

$$\delta\varphi^{\pm}(x,\omega) = \sum_n \delta\varphi_n^{\pm}(x)\delta(\omega - n\omega_0), \tag{47}$$

where the components $\delta\varphi_n^{\pm}(x)$ satisfy

$$\mathcal{B}_n\delta\varphi_n^{\pm}(x) = -\delta\mathcal{B}_n\varphi_c^{\pm}(x), \tag{48}$$

which can be solved separately for each $n \geq 1$ (Sanchez, 2015; Rouchon, 2016). In practice, instead of working with complex variables we will further decompose the operators and the noise into real and imaginary parts, which is the strategy adopted by most numerical solvers for the Fourier-domain linearized noise equations, either deterministic or Monte Carlo (Rouchon, 2016).

To fix the ideas, we will consider a rod composed of three regions: a centrally located fuel pin within the inner boundaries at $x = x_l$ and $x = x_r$, and a host moderator in $x \leq x_l$ and $x \geq x_r$, as illustrated in Fig. 2. This configuration is inspired by the Colibri experimental setup, developed in the framework of the CORTEX project, where one or several fuel rods of the Crocus zero-power pool-type reactor are oscillated at different frequencies for the purpose of neutron noise analysis (Lamirand et al., 2020). The physical parameters for the three regions are the following: for the moderator, we take $\Sigma_s = 3$ cm^{-1} and $\Sigma_c = 0.2$ cm^{-1}; for the fuel, we take $\Sigma_s = 1$ cm^{-1}, $\Sigma_c = 1.2$ cm^{-1} and $\Sigma_f = 0.98$ cm^{-1}. The delayed neutron fraction is $\beta = 7 \times 10^{-3}$ and the precursor decay constant is $\lambda = 0.08$ s^{-1}. The neutron speed is $\upsilon = 2.2 \times 10^5$ cm/s. For our simulations, we will consider three symmetrical configurations with a decreasing size d for the fuel region, and the average number $\nu_t = \nu_p + \nu_d$ of fission neutrons will be adjusted in order to make the system critical: for the first, we take $d = 6$ cm, with $x_l = 2$ cm and $x_r = 8$ cm, and $\nu_t = 2.2711$; for the second, $d = 4$ cm, with $x_l = 3$ cm and $x_r = 7$ cm, and $\nu_t = 2.30635$; for the third, $d = 2$ cm, with $x_l = 4$ cm and $x_r = 6$ cm, and $\nu_t = 2.4250$. In all cases, the total segment length is $L = 10$ cm and the number of spatial meshes for numerical integration is 8000. The corresponding fundamental modes φ_c, normalized to unit, are shown in Fig. 3.

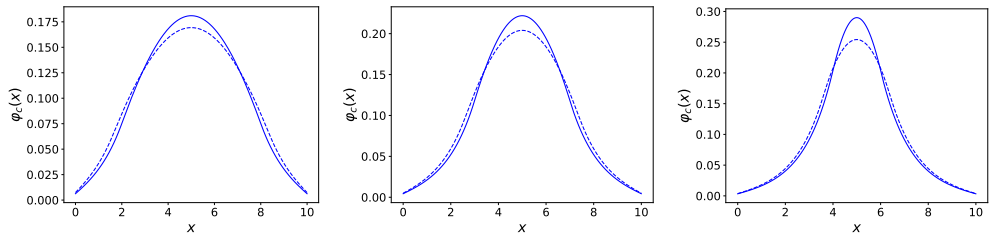

Figure 3: Stationary solution for the rod model with a central fuel rod in a host moderator. Solid lines: the critical flux $\varphi_c(x)$. Dashed lines: the critical flux $\hat{\varphi}_c(x)$ with average correction, as detailed in Sec. 5.4. Left: fuel region size $d = 6$ cm; center: $d = 4$ cm; right: $d = 2$ cm.

As for the perturbation, we will assume that the forcing frequency is $\omega_0/2\pi = 0.1$ Hz, with a vibration amplitude $\varepsilon = 0.5$ cm, unless otherwise specified.

4.1. A single vibrating interface

We start our analysis by considering the somewhat artificial case of a single vibrating interface located at the right boundary of the fuel region ($x = x_r$). The main findings obtained from the application of the linearized equations coupled to the exact model of the noise source or to the ε/d approximation are illustrated in Figs. 4-6 for the configuration with $d = 4$ cm. We have computed the first four components, from ω_0 to $4\omega_0$. It turns out that the noise field $\delta\varphi(x,\omega)$ is dominated by the components corresponding to the first and the second harmonic: this is due to the shape of the noise source, the first and the second harmonic having the smallest number of nodes, and thus the smallest compensation effects between positive and negative contributions. Thus, the noise field for $3\omega_0$ and $4\omega_0$ will not be displayed.

Concerning the noise source, the real part of $Q(x,\omega)$ is dominated by the component due to $2\omega_0$, whereas the imaginary part of $Q(x,\omega)$ is dominated by the component due to ω_0. The real part of $\delta\varphi$ due to ω_0 has approximately the same amplitude as the one due to $2\omega_0$, but opposite sign. On the contrary, the imaginary part of $\delta\varphi$ due to ω_0 is considerably larger than the one due to $2\omega_0$. This behaviour is mirrored in the shape of the absolute value of $\delta\varphi$ (Fig. 6): an hypothetical noise detector would show a peak at ω_0 whose intensity would be much stronger than at $2\omega_0$ at any spatial location within the rod.

An interesting observation is that the ε/d approximation yields an accurate estimate for the shape of the noise field, for both the first and the second harmonic, despite some apparent discrepancies concerning the shape of the noise source. Quite surprisingly, this holds true even for our choice of ε, which is somewhat large as compared to the linear size d of the fuel region.

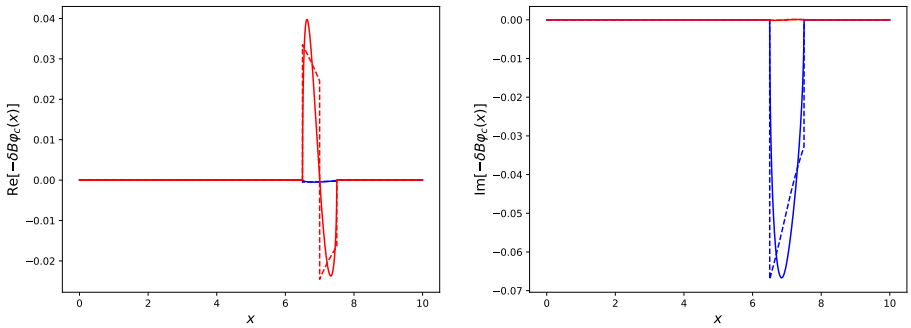

Figure 4: The noise source $Q(x,\omega)$ for a single vibrating interface at $x_r = 7$. Left: real part; right: imaginary part. Blue: harmonic component for ω_0; red: $2\omega_0$. Solid lines: exact source model; dashed lines: ϵ/d approximation.

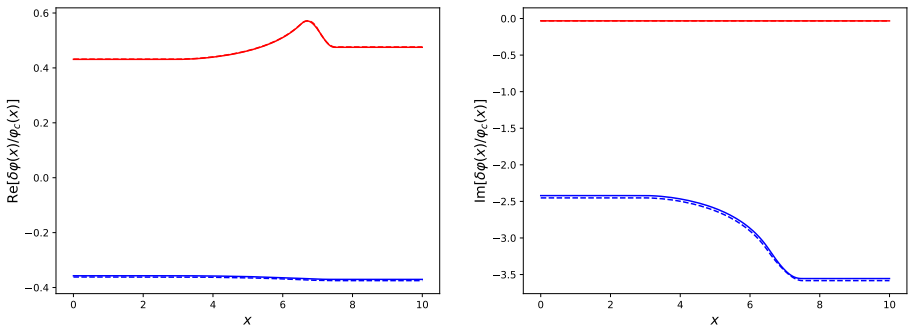

Figure 5: The normalized noise field for a single vibrating interface at $x_r = 7$. Left: real part; right: imaginary part. Blue: harmonic component for ω_0; red: $2\omega_0$. Solid lines: exact source model; dashed lines: ϵ/d approximation.

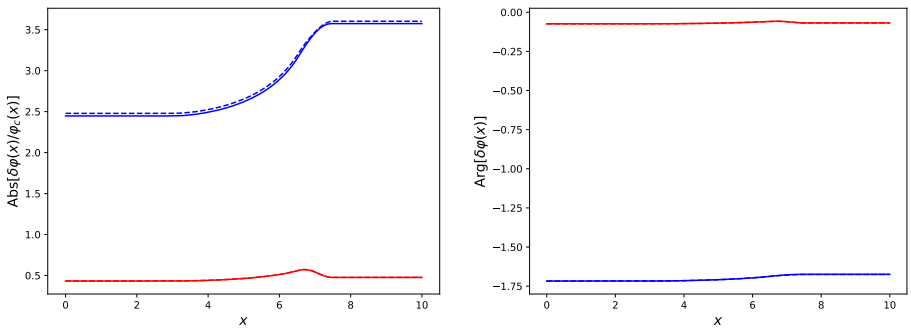

Figure 6: The normalized noise field for a single vibrating interface at $x_r = 7$. Left: amplitude; right: phase. Colors and line styles are the same as in Fig. 5.

4.2. Two vibrating interfaces

We discuss next the more physical case of two interfaces vibrating in phase at each end of the fuel region, each giving rise to the shapes discussed in Sec. 4.1, but with opposite signs because of $\Delta\Sigma_\alpha$, which would mimic the effect of the fuel pin being oscillated into the moderator. The main simulation results obtained from the application of the linearized equations coupled to the exact model of the noise source or to the ε/d approximation are illustrated in Figs. 7-9 for the configuration with $d = 6$ cm, in Figs. 10-12 for the configuration with $d = 4$ cm, and in Figs. 13-15 for the configuration with $d = 2$ cm. The computed noise field for $3\omega_0$ and $4\omega_0$ is again negligible with respect to that of the first two harmonics and will not be displayed.

As expected, at each interface the qualitative behaviour of the noise source is similar to the case of the source corresponding to a single interface (see Figs. 7, 10 and 13). The real part of $Q(x,\omega)$ is dominated by the component due to $2\omega_0$, whereas the imaginary part of $Q(x,\omega)$ is dominated by the component due to ω_0. However, the corresponding noise field $\delta\varphi(x,\omega)$ has a distinct shape, because of the linear superposition of the noise sources, which results in non-trivial interference effects. The real part of $\delta\varphi(x,\omega)$ is dominated by the component due to $2\omega_0$ (Figs. 8, 11 and 14, left), which is symmetric with respect to the two interfaces and thus leads to a constructive interference; for the same cases, the contribution of ω_0 to the real part is on the contrary suppressed by a destructive interference. Conversely, the imaginary part of $\delta\varphi(x,\omega)$ is dominated by the component due to ω_0, which is anti-symmetric with respect to the two interfaces, and thus leads to a destructive interference (Figs. 8, 11 and 14, right). Observe in particular that the imaginary noise component due to ω_0 has now a node at $x = L/2$, corresponding to the mid-point of the two interfaces. This behaviour is mirrored in the shape of the amplitude of $\delta\varphi(x,\omega)$ (Figs. 9, 12 and 15, left): the component due to ω_0 is larger than the one due to $2\omega_0$ far from the vibrating region; conversely, the component due to $2\omega_0$ becomes larger than the one due to ω_0 within the vibrating region, where the first harmonic is suppressed. Again, the ε/d approximation yields an accurate estimate for the shape of the noise field, for both the first and the second harmonic.

The linear separation d between x_l and x_r has a strong impact on the behaviour of the noise field. When reducing the size d of the fuel region by keeping fixed the amplitude ε of the vibration, a striking phenomenon occurs: the real part of $\delta\varphi$ corresponding to the component due to $2\omega_0$ increases dramatically (Figs. 8, 11 and 14, left) and so does the corresponding amplitude of the noise field (Figs. 9, 12 and 15, left). Since the component due to ω_0 is comparatively

much less sensitive to d, the amplitude of the noise field corresponding to the second harmonic may become everywhere larger (and eventually much larger) than the one corresponding to the first harmonic, provided that the separation d of the two interfaces is sufficiently small (see Fig. 15, left, for the configuration with $d = 2$ cm). According to the linearized equations, an hypothetical noise detector would thus show a peak at $2\omega_0$ whose intensity would be much stronger than at ω_0 at any location within the rod. The same behaviour is observed when increasing the size of ε for a given d. These surprising features are consistent with the recent findings related to Monte Carlo simulations of the linearized noise equations mentioned before. In general, we would expect that a linear system under the effect of an external forcing function at a frequency ω_0 should primarily respond at the same frequency, except for special cases where the symmetries of the forcing function and/or the detectors might suppress the response at ω_0 and thus artificially promote the response at $2\omega_0$. One then wonders whether the predictions of the linear theory in the Fourier domain are physically sound for the configurations examined here.

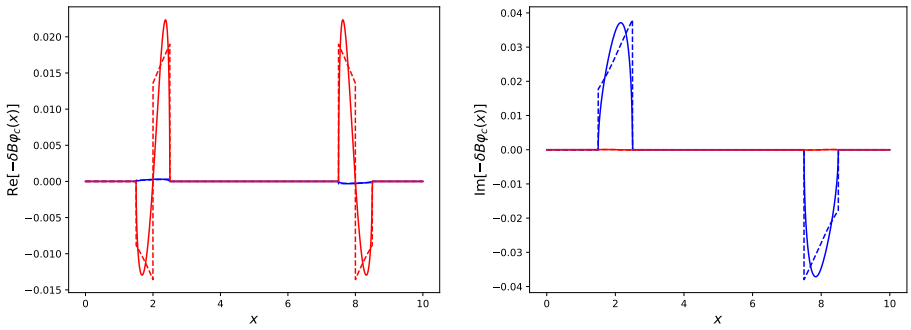

Figure 7: The noise source $Q(x, \omega)$ for two vibrating interfaces with $d = 6$ cm. Left: real part; right: imaginary part. Blue: harmonic component for ω_0; red: $2\omega_0$. Solid lines: exact source model; dashed lines: ϵ/d approximation for ω_0 and $2\omega_0$.

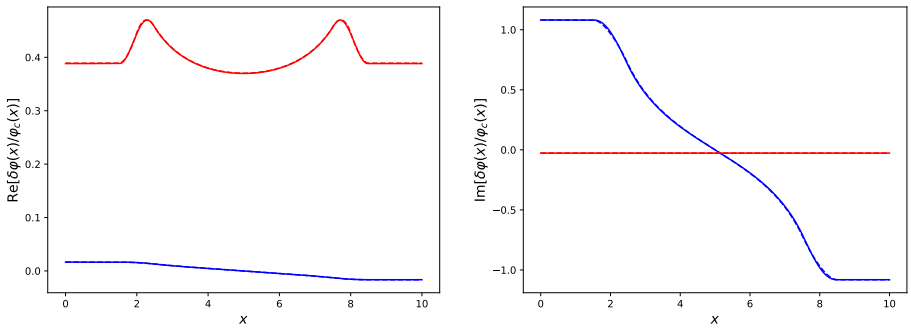

Figure 8: The normalized noise field for two vibrating interfaces with $d = 6$ cm. Left: real part; right: imaginary part. Blue: harmonic component for ω_0; red: $2\omega_0$. Solid lines: exact source model; dashed lines: ϵ/d approximation for ω_0 and $2\omega_0$.

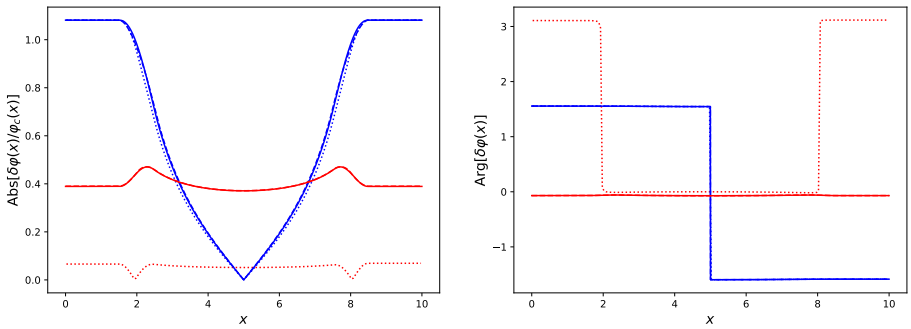

Figure 9: The normalized noise field for two vibrating interfaces with $d = 6$ cm. Left: amplitude; right: phase. Colors and line styles are the same as in Fig. 8. Additionally, reference solutions obtained by solving the time-dependent equations, as described in Sec. 5.1, are plotted as dotted lines.

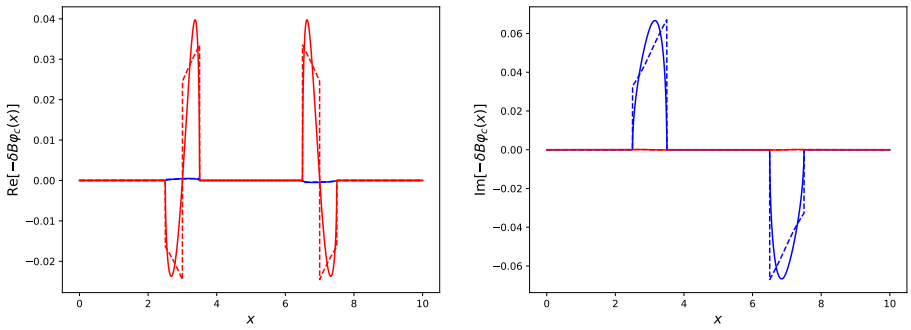

Figure 10: The noise source $Q(x, \omega)$ for two vibrating interfaces with $d = 4$ cm. Left: real part; right: imaginary part. Blue: harmonic component for ω_0; red: $2\omega_0$. Solid lines: exact source model; dashed lines: ϵ/d approximation for ω_0 and $2\omega_0$.

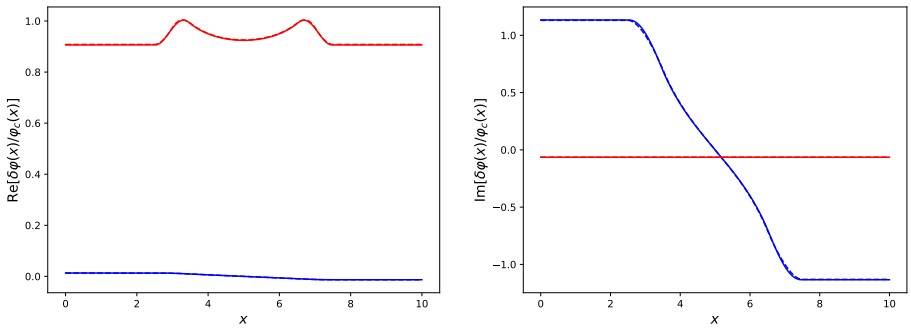

Figure 11: The normalized noise field for two vibrating interfaces with $d = 4$ cm. Left: real part; right: imaginary part. Blue: harmonic component for ω_0; red: $2\omega_0$. Solid lines: exact source model; dashed lines: ϵ/d approximation for ω_0 and $2\omega_0$.

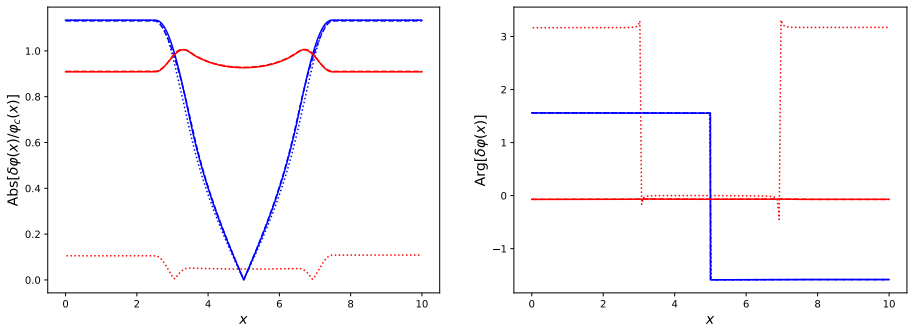

Figure 12: The normalized noise field for two vibrating interfaces with $d = 4$ cm. Left: amplitude; right: phase. Colors and line styles are the same as in Fig. 11. Additionally, reference solutions obtained by solving the time-dependent equations, as described in Sec. 5.1, are plotted as dotted lines.

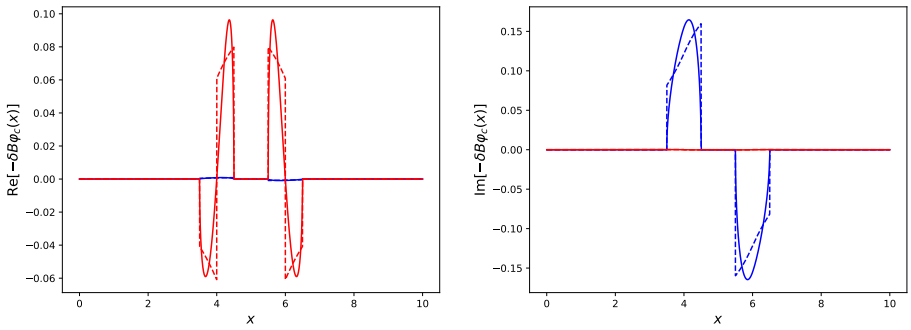

Figure 13: The noise source $Q(x, \omega)$ for two vibrating interfaces with $d = 2$ cm. Left: real part; right: imaginary part. Blue: harmonic component for ω_0; red: $2\omega_0$. Solid lines: exact source model; dashed lines: ϵ/d approximation for ω_0 and $2\omega_0$.

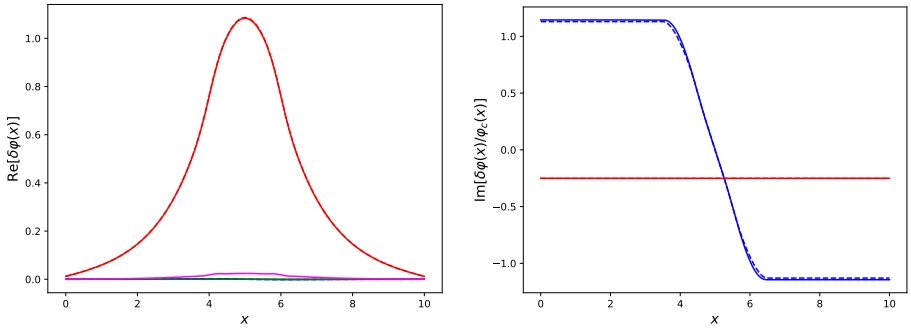

Figure 14: The normalized noise field for two vibrating interfaces with $d = 2$ cm. Left: real part; right: imaginary part. Blue: harmonic component for ω_0; red: $2\omega_0$. Solid lines: exact source model; dashed lines: ϵ/d approximation for ω_0 and $2\omega_0$.

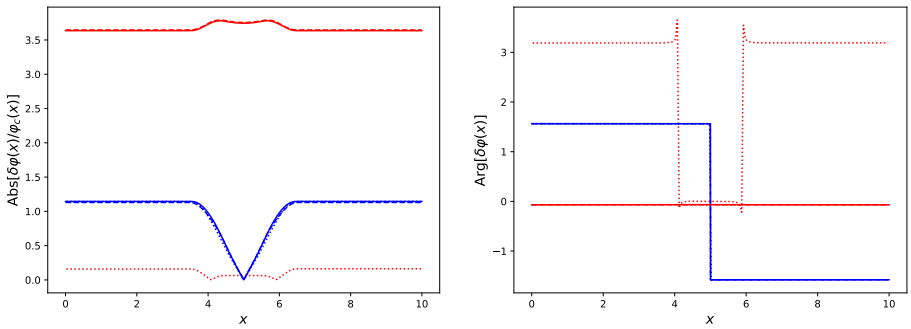

Figure 15: The normalized noise field for two vibrating interfaces with $d = 2$ cm. Left: amplitude; right: phase. Colors and line styles are the same as in Fig. 14. Additionally, reference solutions obtained by solving the time-dependent equations, as described in Sec. 5.1, are plotted as dotted lines.

5. Non-perturbative approach to the noise equations

In order to ascertain whether the linearized noise equations in the Fourier domain provide a faithful representation of the system behaviour in the presence of vibrating boundaries, reference solutions are required. For this purpose, we analyze the rod problem using a time-domain solver, the non-perturbative equations in the Fourier domain, and finally an average-corrected version of the non-perturbative equations in which a compensation is included for the possible reactivity effect.

5.1. Reference solutions from a time-domain solver

We have developed a time-domain solver for the time-dependent rod model equations, namely,

$$\left[\frac{1}{\upsilon}\frac{\partial}{\partial t} \pm \frac{\partial}{\partial x} + \Sigma_t(x,t)\right]\varphi^{\pm}(x,t) = \frac{1}{2}\left[\Sigma_s(x,t) + \frac{\nu_p\Sigma_f(x,t)}{k_{\text{eff}}}\right]\varphi(x,t) + \frac{1}{2}\lambda c(x,t)$$
$$\frac{\partial}{\partial t}c(x,t) = \frac{\nu_d\Sigma_f(x,t)}{k_{\text{eff}}}\varphi(x,t) - \lambda c(x,t), \tag{49}$$

where $\varphi^{\pm}(x,t)$ is the angular flux and $\varphi(x,t) = \varphi^{+}(x,t) + \varphi^{-}(x,t)$ is the scalar flux integrated over the directions. The viable space is again the segment $[0,L]$, with leakage boundary conditions $\varphi^{+}(0,t) = 0$ and $\varphi^{-}(L,t) = 0$. The initial conditions for Eq. (49) correspond to a critical state:

$$c(x,0) = \frac{1}{\lambda}\frac{\nu_d\Sigma_f(x,0)}{k_{\text{eff}}}\varphi(x,0), \tag{50}$$

where $\varphi(x,0) = \varphi_c(x)$ is the reactor fundamental mode. The functional behaviour of the time-dependent cross sections for reaction α is given by

$$\delta\Sigma_\alpha(x,t) = \Delta\Sigma_\alpha\left[H(x-x_0) - H(x-x_0-\varepsilon\sin(\omega_0 t))\right], \tag{51}$$

where $\Delta\Sigma_\alpha = \Sigma_\alpha^L - \Sigma_\alpha^R$ is the difference between the spatially homogeneous cross sections at the left and the right of each interface located at x_0.

Since the system of equations in (49) is stiff because of the large separation between the typical time scale of the neutrons and the one of the precursors, in order to determine the behaviour of the angular flux $\varphi^{\pm}(x,t)$ the precursor equation has been discretized in time by using an explicit Euler scheme, whereas the Boltzmann equation for the neutrons has been discretized by using a backward Euler method (Vidal-Ferrándiz et al., 2020). The equations are integrated over

a domain $[0, T]$, starting from the equilibrium conditions at $t = 0$. For our examples, we have taken $T = 500$ s. Once the scalar neutron field $\varphi(x, t)$ has been determined at a collection of hypothetical detectors located at several spatial locations $0 \leq x_j \leq L$ within the domain, the neutron noise field is then obtained by taking

$$\delta\varphi(x_j, t) = \frac{\varphi(x_j, t) - \varphi_c(x_j)}{\varphi_c(x_j)}. \tag{52}$$

Finally, the Fourier-transformed neutron noise field is computed by taking the FFT of the expression derived in Eq. (52), over the discrete grid of times $0 \leq t_i \leq T$ for which the time-dependent noise field is available, and for each spatial location x_j. We will thus have reference solutions for the noise field within the system, to be compared with the results stemming from the linearized equation (45) in the Fourier domain. For the calculations described here, we have chosen 400 locations x_j, evenly distributed in $[0, L]$.

The simulation findings are illustrated in Fig. 9 for $d = 6$ cm, Fig. 12 for $d = 4$ cm, and Fig. 15 for $d = 2$ cm. For the first harmonic, the amplitude and the phase of noise field stemming from the linearized noise equations in the Fourier domain are in good agreement with the reference solution obtained by integrating the kinetic equations. However, for the second harmonic the linearized noise equations completely fail to address the features of the amplitude and the phase, regardless of the use of the exact model or the ε/d model for the noise source: the phase should have a step-wise variation within the vibrating region, and the amplitude should be much smaller. In particular, the abrupt increase of the second harmonic for small d seems to be an artefact induced by the orthodox linearization.

5.2. Non-perturbative equations in the Fourier domain

For the benchmark configurations discussed in this work, the reference solutions obtained from the time-domain analysis suggest that the linear approximation in the Fourier domain is appropriate for the first harmonic, but is not capable of reproducing the key properties of the amplitude and phase of the noise field for the second harmonic. In this Section we will explore the impact of the non-perturbative noise equations (43) on the accuracy of the system response in the Fourier domain.

In practice, a numerical solution of Eq. (43) requires a truncation of the infinite sum over m, which can be obtained by applying a cut-off at $m = \pm M$: this leads to a closed system, containing only terms for which an explicit equation is available. This system can be solved by iteration as follows (Sanchez, 2015;

Rouchon and Sanchez, 2015; Rouchon, 2016): first, we solve the linearized problem

$$\mathcal{B}_n \delta\varphi_n^{(0)} = -\delta\mathcal{B}_n \varphi_c, \tag{53}$$

in order to initialize the noise field $\delta\varphi_n^{(0)}$ for each frequency component $n\omega_0$; then, for each iteration $j \geq 1$ we compute the effective noise source

$$Q_n^{(j)}(\omega) = -\delta\mathcal{B}_n \varphi_c - \frac{1}{2\pi} \sum_{m \neq n} \delta\mathcal{B}_{n-m} \delta\varphi_m^{(j-1)}; \tag{54}$$

finally, the noise field is determined by solving

$$\left[\mathcal{B}_n + \frac{1}{2\pi} \delta\mathcal{B}_0 \right] \delta\varphi_n^{(j)} = Q_n^{(j)}(\omega). \tag{55}$$

This procedure is iterated until appropriate convergence criteria on the norm $\|\delta\varphi_n^{(j)} - \delta\varphi_n^{(j-1)}\|$ are met. At convergence, $j \to \infty$, the noise field $\delta\varphi_n^{(\infty)}$ formally satisfies a linearized equation where the operator $\mathcal{B}_n$ is replaced by the modified operator $\mathcal{B}_n + \delta\mathcal{B}_0/2\pi$ and the source $-\delta\mathcal{B}_n\varphi_c$ is replaced by the effective source $Q_n^{(\infty)}(\omega)$. The term $\delta\mathcal{B}_0$ is kept on the left hand side of the equation: numerical investigations have shown that such operator shift can contribute to the stability of the iterations (Mancusi and Zoia, 2018). Since the equations are coupled, the components at each frequency $n\omega_0$ will also depend on $\delta\varphi_0$, which is related to the reactivity offset and was dropped in the linearized equations: this term will need a distinct treatment, as shown in the following.

5.3. The rod model revisited

Based on the analysis of the linear system, it appears that the two major contributors to the behaviour of the noise field are ω_0 and $2\omega_0$, the components corresponding to $n \geq 3$ being small for the configurations considered in this work. We can thus safely assume that the dominant portion of the corrections due to the convolution term in Eq. (43) will be carried by $\delta\varphi_1$ and $\delta\varphi_2$, and choose the cut-off $M = 4$. For the time being, we also neglect the component at $\omega = 0$ by artificially setting $\delta\varphi_0 = 0$.

We revisit then the rod model with two vibrating interfaces. The convergence of the non-perturbative corrections is achieved in about 20 iterations for $d = 6$ cm, 30 iterations for $d = 4$ cm and 70 iterations for $d = 2$ cm. The numerical solutions for the non-perturbative noise equations are compared to those of the linearized equations in Figs. 16-18 for the configuration with $d = 6$, Figs. 19-21 for the configuration with $d = 4$ cm, and Figs. 22-24 for the configuration with $d = 2$

cm. Concerning the effective noise source, the component at $2\omega_0$ is slightly but systematically affected by the additional terms given by the convolution product, whereas the component at ω_0 is almost unaffected (Figs. 16, 19 and 22).

Despite these modifications of the effective source being rather small, the corresponding impact on the noise field is extremely strong, which shows that the symmetry-induced compensations occurring in linearized equations are broken by the presence of the coupling terms of the non-perturbative equations. In particular, the real part of the second harmonic is dramatically decreased with respect to the linearized noise equations (Figs. 17, 20 and 23, left), which in turn is mirrored by a decrease of the amplitude of this harmonic (Figs. 18, 21 and24, left). Conversely, the component due to ω_0 is minimally modified by the non-perturbative terms. Eventually, within the framework of the non-perturbative noise equations the first harmonic dominates everywhere, except for the vibrating region, where the absolute value of $\delta\varphi_1(x)$ is depressed because of the anti-symmetry of the imaginary part of the component due to ω_0.

The noise fields obtained by using the non-perturbative equations have been compared to the reference solutions in Figs. 18, 21 and 24. For the first harmonic, the corrections due to the non-perturbative terms are rather small, and the overall agreement with respect to the reference solutions are good, except for the case of the smallest fuel region ($d = 2$ cm), where a slight but systematic discrepancy is found far from the vibrating region. On the contrary, the impact of the non-perturbative terms on the second harmonic is very strong: for all the tested configurations, the non-linearized noise equations perform better than the linearized equations in reproducing the spatial behaviour of the second harmonic, for both amplitude and phase (compare Figs. 18, 21 and 24 against Figs. 9, 12 and 15, respectively). However, for decreasing d the discrepancy with respect to the reference solution tends to increase. This is particularly apparent for the configuration with $d = 2$ cm: while for the other configurations the non-perturbative equations were able to correctly reproduce the phase jump of the second harmonic within the vibrating region (which the linearized equations failed to do), for this case the predicted phase is spatially flat, and the shape of the amplitude is correspondingly far from the reference curve. The origin of such discrepancies will be investigated in the next section.

5.4. Average-corrected noise equations

In the customary derivation of the noise equations, the neutron noise is defined as the time-dependent deviation with respect to the steady-state flux φ_c satisfying Eq. (1). This hypothesis underlies the entire formalism for both the linearized and the non-perturbative noise equations in the Fourier domain. Actually,

some recent works have suggested that the traditional decomposition of the time-dependent neutron flux as in Eq. (4) might not be the wisest choice (Sanchez, 2015; Rouchon and Sanchez, 2015; Rouchon, 2016). The neutron flux φ_c corresponds to the initial condition of the system, before the perturbation is introduced; once the perturbation is effective, the net reactivity induced by the perturbation will be compensated by control rod adjustments, physical feedbacks such as Doppler effect, or any other external control mechanisms, which will prevent the system from drifting, and the reactor will asymptotically reach a new steady state $\hat{\varphi}_c \neq \varphi_c$. In order to mimic these effects, we will simply assume that the average number of fission neutrons is rescaled by $\hat{k}_{\text{eff}}$ (Sanchez, 2015), where $\hat{k}_{\text{eff}} \neq k_{\text{eff}}$ is the new fundamental eigenvalue associated to the steady state including the perturbation (Sanchez, 2015; Rouchon and Sanchez, 2015; Rouchon, 2016).

Correspondingly, we will define the neutron noise $\delta\hat{\varphi}$ as

$$\hat{\varphi}(\mathbf{r}, \mathbf{\Omega}, E, t) = \hat{\varphi}_c(\mathbf{r}, \mathbf{\Omega}, E) + \delta\hat{\varphi}(\mathbf{r}, \mathbf{\Omega}, E, t), \tag{56}$$

which ensures that the noise will have a time-average equal to zero, i.e.,

$$\langle \delta\hat{\varphi} \rangle \equiv \lim_{T\to\infty} \frac{1}{2T} \int_{-T}^{T} \delta\hat{\varphi}(\mathbf{r}, \mathbf{\Omega}, E, t) dt = 0, \tag{57}$$

where we have used the short-hand notation $\langle \cdot \rangle$ for the time average. This procedure allows rigorously having $\delta\hat{\varphi}_0 = \delta\hat{\varphi}(\omega = 0) = 0$, which minimizes the possible bias in the non-perturbative equations due to having artificially set $\delta\varphi_0 = 0$ in the previous section.

For this purpose, we decompose the perturbed Boltzmann operator as

$$\mathcal{B}_p = \hat{\mathcal{B}}(t) + \delta\hat{\mathcal{B}}(t), \tag{58}$$

and we set

$$\hat{\mathcal{B}}(t) = \mathcal{B}(t) + \mathcal{A} \tag{59}$$

and

$$\delta\hat{\mathcal{B}}(t) = \delta\mathcal{B}(t) - \mathcal{A}, \tag{60}$$

where $\mathcal{A}$ is a suitable time-independent operator, to be determined. We further require $\hat{\varphi}_c$ to satisfy the eigenvalue equation $\hat{\mathcal{B}}_c\hat{\varphi}_c = 0$, where $\hat{\mathcal{B}}_c$ is the stationary operator associated to $\hat{\mathcal{B}}(t)$. The resulting noise equation in the time domain reads

$$\left[\hat{\mathcal{B}}(t) + \delta\hat{\mathcal{B}}(t)\right] \delta\hat{\varphi}(t) = -\delta\hat{\mathcal{B}}(t)\hat{\varphi}_c, \tag{61}$$

which can be then Fourier-transformed to yield

$$\hat{\mathcal{B}}_n \delta\hat{\varphi}_n + \frac{1}{2\pi}\sum_m \delta\hat{\mathcal{B}}_{n-m}\delta\hat{\varphi}_m = -\delta\hat{\mathcal{B}}_n\hat{\varphi}_c \tag{62}$$

for the noise components at discrete frequencies $n\omega_0$. Then, a sufficient (albeit non-unique) condition to ensure that $\delta\hat{\varphi}_0 = 0$ is

$$\mathcal{A}\hat{\varphi}_c = \delta\mathcal{B}_0\hat{\varphi}_c + \frac{1}{2\pi}\sum_m \delta\hat{\mathcal{B}}_{-m}\delta\hat{\varphi}_m. \tag{63}$$

Thus, we formally set the operator $\mathcal{A}$ to be (Sanchez, 2015)

$$\mathcal{A} \equiv \delta\mathcal{B}_0 + \frac{1}{2\pi}\sum_m \delta\hat{\mathcal{B}}_{-m}\frac{\delta\hat{\varphi}_m}{\hat{\varphi}_c}. \tag{64}$$

Since $\mathcal{A}$ depends on $\hat{\varphi}_c$ and $\delta\hat{\varphi}_n$, which are the solutions of the problem that we are attempting to solve, an iterative strategy must be used in order to determine the noise field corresponding to the average-corrected non-perturbative noise equations (Rouchon and Sanchez, 2015; Rouchon, 2016). We first solve the non-perturbative noise equations without taking into account the average correction, as detailed in Sec. 5.2, and estimate $\delta\varphi_n$. Then, we determine $\mathcal{A}$ based on Eq. (64) and compute the modified operators $\hat{\mathcal{B}}_n$ and $\delta\hat{\mathcal{B}}_n$ in the Fourier domain. This allows computing the new steady-state flux $\hat{\varphi}_c$ and successively updating the noise field $\delta\hat{\varphi}_n$. By iterating these steps, this procedure eventually converges towards the average-corrected $\delta\hat{\varphi}_n$ satisfying $\delta\hat{\varphi}_0 = 0$.

We have numerically assessed the impact of using the average-corrected noise equations for the benchmark examples considered above. The corresponding average-corrected stationary fluxes $\hat{\varphi}_c(x)$ are contrasted to the respective $\varphi_c(x)$ in Fig. 3. The solutions of the average-corrected noise equations converge in about 10 external iterations for the operators. The main findings for the resulting noise fields $\delta\hat{\varphi}_n$ are then illustrated in Figs. 16-18 for the configuration with $d = 6$ cm, Figs. 19-21 for the configuration with $d = 4$ cm, and Figs. 22-24 for the configuration with $d = 2$ cm. For the first harmonic, the average-corrected equations show only slight deviations as compared to the previous analysis for $d = 6$ cm and $d = 4$ cm; nonetheless, for the case $d = 2$ cm the average-corrected equations considerably improve the agreement with the reference solution, especially outside the vibrating region. The overall conclusion is that the noise equations for the first harmonic are rather robust, in the sense that the linearized, non-

perturbative and average-corrected equations yield almost identical predictions concerning the shape of the noise field. For the second harmonic, on the other hand, the average-corrected equations are key in reducing the bias with respect to the reference solution: the phase shift within the vibrating region and the spatial shape of the noise field of the amplitude are correctly recovered, even for the case $d = 2$ cm. Slight residual discrepancies between the Fourier-domain noise equations and the reference solutions can be attributed to the numerical accuracy of the time integration, to the discretization error of both the time and frequency domain approaches, and to the truncation to the order M in the treatment of the non-perturbative equations.

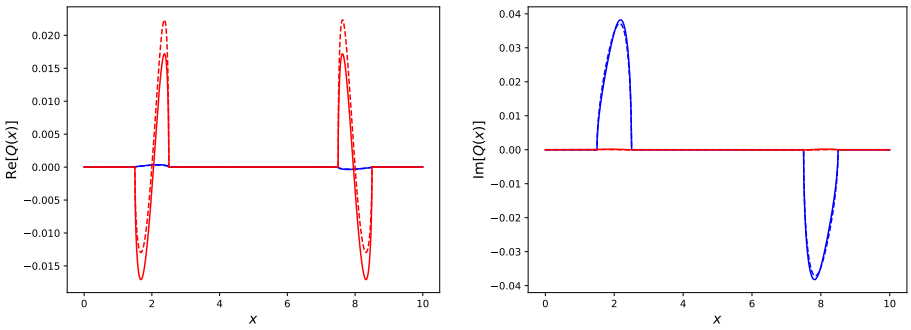

Figure 16: The noise source $Q(x, \omega)$ for two vibrating interfaces with $d = 6$ cm. Left: real part; right: imaginary part. Blue: harmonic component for ω_0; red: $2\omega_0$. Solid lines: non-perturbative equations; dashed lines: linearized equations.

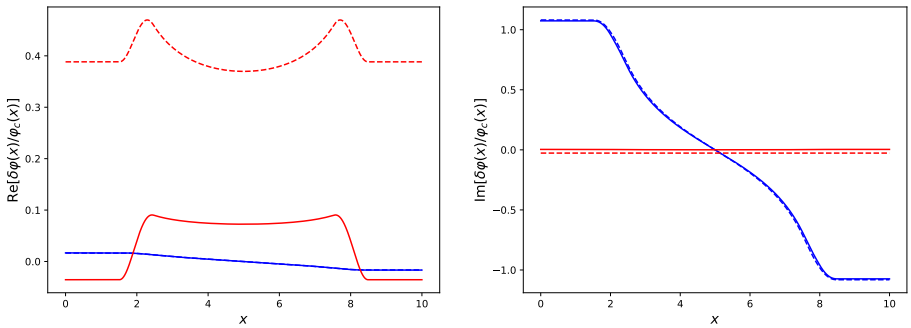

Figure 17: The normalized noise field for two vibrating interfaces with $d = 6$ cm. Left: real part; right: imaginary part. Blue: harmonic component for ω_0; red: $2\omega_0$. Solid lines: non-perturbative equations; dashed lines: linearized equations.

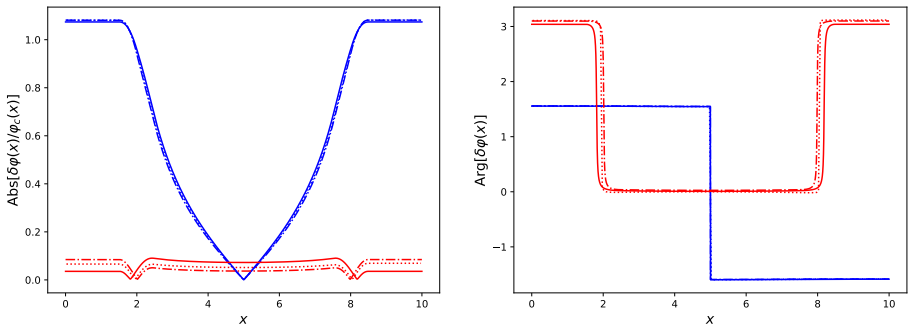

Figure 18: The normalized noise field for two vibrating interfaces with $d = 6$ cm. Left: amplitude; right: phase. Solid lines: non-perturbative equations (Sec. 5.2); dotted lines: reference solution from the time-domain solver (Sec. 5.1); dotted-dashed lines: non-perturbative equations with average correction (Sec. 5.4).

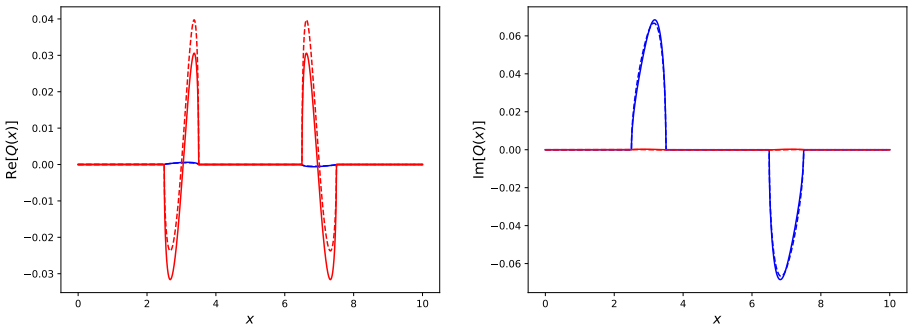

Figure 19: The noise source $Q(x, \omega)$ for two vibrating interfaces with $d = 4$ cm. Left: real part; right: imaginary part. Blue: harmonic component for ω_0; red: $2\omega_0$. Solid lines: non-perturbative equations; dashed lines: linearized equations.

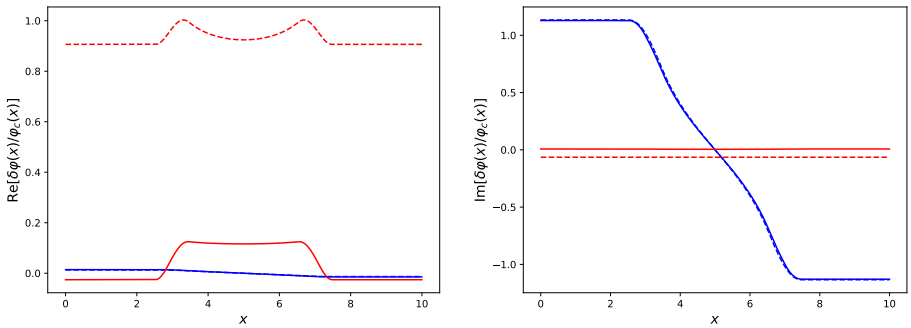

Figure 20: The normalized noise field for two vibrating interfaces with $d = 4$ cm. Left: real part; right: imaginary part. Blue: harmonic component for ω_0; red: $2\omega_0$. Solid lines: non-perturbative equations; dashed lines: linearized equations.

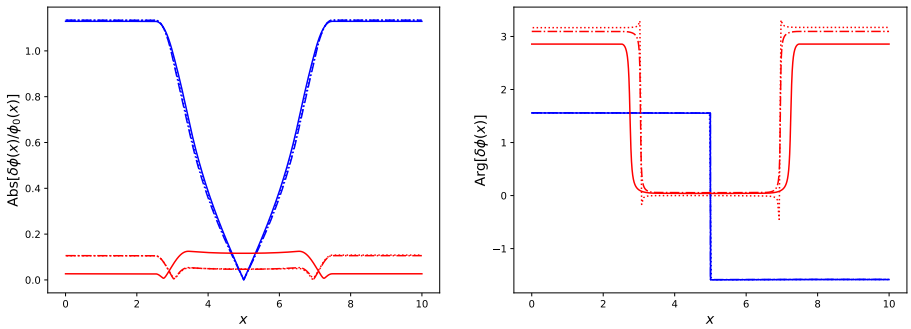

Figure 21: The normalized noise field for two vibrating interfaces with $d = 4$ cm. Left: amplitude; right: phase. Solid lines: non-perturbative equations (Sec. 5.2); dotted lines: reference solution from the time-domain solver (Sec. 5.1); dotted-dashed lines: non-perturbative equations with average correction (Sec. 5.4).

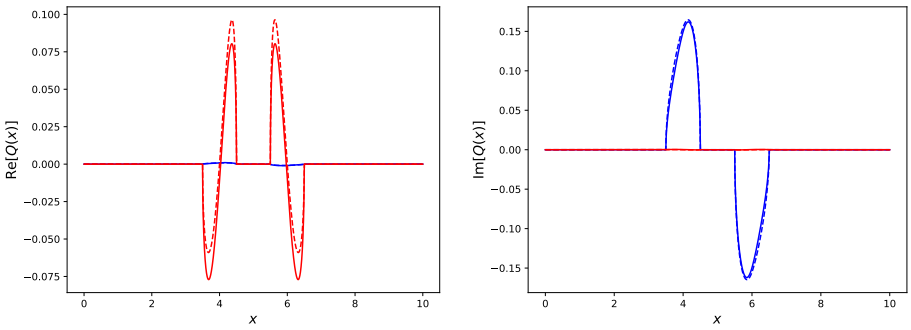

Figure 22: The noise source $Q(x, \omega)$ for two vibrating interfaces with $d = 2$ cm. Left: real part; right: imaginary part. Blue: harmonic component for ω_0; red: $2\omega_0$. Solid lines: non-perturbative equations; dashed lines: linearized equations.

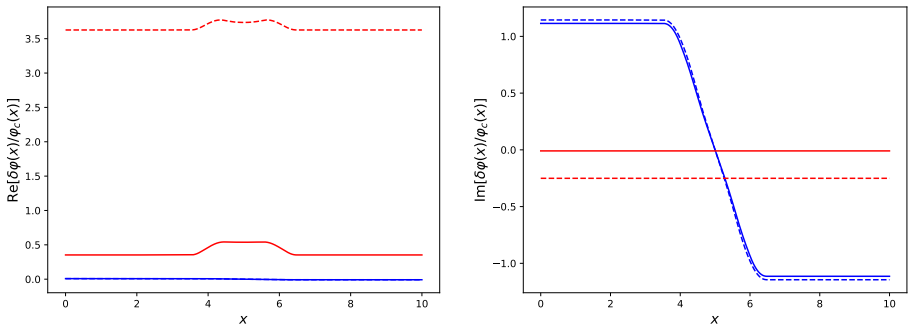

Figure 23: The normalized noise field for two vibrating interfaces with $d = 2$ cm. Left: real part; right: imaginary part.Blue: harmonic component for ω_0; red: $2\omega_0$. Solid lines: non-perturbative equations; dashed lines: linearized equations.

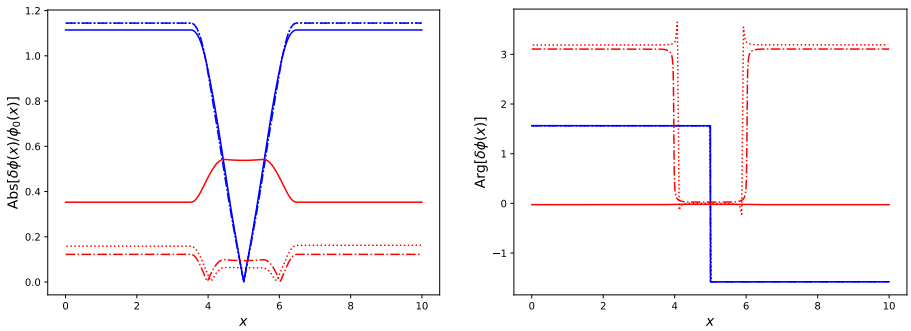

Figure 24: The normalized noise field for two vibrating interfaces with $d = 2$ cm. Left: amplitude; right: phase. Solid lines: non-perturbative equations (Sec. 5.2); dotted lines: reference solution from the time-domain solver (Sec. 5.1); dotted-dashed lines: non-perturbative equations with average correction (Sec. 5.4).

6. Conclusions

In this work we have analyzed the behaviour of the neutron noise equations for a simple benchmark configuration consisting in a fuel rod periodically vibrating at the fundamental frequency ω_0 in a host moderator. In this framework, we have elucidated how the role of the noise source, and in particular the impact of the higher-order terms, is entangled with the structure of the noise equations. We have shown that the non-perturbative noise equations (as opposed to the widely used linearized noise equations) are in some case mandatory in order for the Fourier-domain analysis to be consistent with the reference solutions obtained by solving the time-dependent transport equations. A further improvement comes from the use of the average-corrected noise equations, which can take into account the reactivity offset due to the presence of the perturbation. The discrepancy between the predictions of these three families of noise equations (linearized, non-perturbative and average-corrected) depends on the noise component $\delta\varphi_n$ to be determined and on the system under investigation. For the benchmark selected in this work, the three equations provide consistent estimates for the spatial shape of the first harmonic $\delta\varphi_1$ at ω_0; however, the differences between the three approaches are dramatic for the second harmonic $\delta\varphi_2$ at $2\omega_0$: the linearized equation might hint that the second harmonic is everywhere larger than the first, which contradicts the reference solution; the non-perturbative equations allow obtaining closer, albeit still not entirely accurate, estimates; the average-corrected equations finally yield spatial shapes in very good agreement with the reference solution.

The analysis carried out in this work seems thus to suggest that the non-perturbative, and even better the average-corrected, noise equations are mandatory in order to properly discriminate the double frequency effect of neutron noise possibly measured in detectors, especially in view of comparing the simulation results to experimental measurements. However, these conclusions hold true for the configurations investigated here, namely a small symmetrical system in which the perturbation is centrally located, and their more broad validity for complex systems (three-dimensional geometries, realistic material compositions and cross sections, and multi-group or continuous-energy transport) should be carefully probed. In this context, an important issue concerns the role of symmetries, as apparent from the following example. For the configuration examined here, the growth of the second harmonic with respect to the first for decreasing d appears to be an artefact of the linearized equations, and disappears when introducing the non-perturbative corrections. However, if we had taken a spatially-integrated detector symmetric with respect to the center of the rod, the

dominant noise component would have been at $2\omega_0$, independently of whether we had used the linearized or non-perturbative equations: since the noise field related to the first harmonic is anti-symmetric with respect to the center of the system, its integral over a symmetric detector is vanishing and the second harmonic would be the only surviving noise component. Similarly, the impact of the non-perturbative corrections on the first and second harmonic, which are intimately related to the behaviour of the fundamental neutron flux within the vibrating region, strongly depends on the symmetries of the system. Future work will be aimed at exploring more general cases, in order to further unveil the features the noise equations.

Acknowledgements

The authors are deeply indebted to Dr. D. Mancusi (CEA/Saclay) for many insightful suggestions and wish to thank Prof. I. Pázsit (Chalmers University) for critical comments. The CORTEX research project has received funding from the Euratom research and training programme 2014-2018 under grant agreement No 754316.

M. Antonopoulos-Domis. Reactivity and neutron density noise excited by random rod vibration. *Annals of Nuclear Energy*, 3:451–459, 1976.

K. Behriguer, G. Kosály, and L. Kostic. Reactivity and neutron density noise excited by random rod vibration. *Annals of Nuclear Energy*, 63:306–318, 1977.

D. Chionis, A. Dokhane, L. Belblidia, H. Ferroukhi, G. Girardin, and A. Pautz. Development and verification of a methodology for neutron noise response to fuel assembly vibrations. *Annals of Nuclear Energy*, 147:107669, 2020.

C. Demazière. CORESIM: a multi-purpose neutronic tool for research and education. *Annals of Nuclear Energy*, 38:2698–2718, 2011.

C. Demazière, P. Vinai, M. Hursin, S. Kollias, and J. Herb. Overview of the CORTEX project. In *Proceedings of Physor2018*, Cancun, Mexico, 2018.

D. N. Fry, J. March-Leuba, and F. J. Sweeney. Use of neutron noise of diagnosis of in-vessel anomalies in light-water reactors. Technical Report ORNL/TM-8774, Oak Ridge National Laboratory, 1986.

J. E. Hoogenboom. The two-direction neutral-particle transport model: A useful tool for research and education. *Transp. Theory Stat. Phys.*, 37:65–108, 2008.

A. Jonsson, H. N. Tran, V. Dykin, and I. Pazsit. Analytical investigation of the properties of the neutron noise induced by vibrationg absorber and fuel rods. *Kerntechnik*, 77:371–380, 2012.

G. Kosály. Noise investigations in boiling-water and pressurized-water reactors. *Progr. Nucl. Energy*, 5:145–199, 1980.

V. Lamirand, P. Frajtag, D. Godat, O. Pakari, A. Laureau, A. Rais, M. Hursin, G. Hursin, C. Fiorina, and A. Pautz. The COLIBRI experimental program in the CROCUS reactor: characterization of the fuel rods oscillator. *EPJ Web Conf.*, 225:04020, 2020.

A. Lucia, E. Ohlmer, and D. Schwalm. Correlation between neutron noise and fuel element oscillations in the ECO reactor. *Atomkernenergie*, 22:6–8, 1973.

D. Mancusi and A. Zoia. Chaos in eigenvalue search methods. *Ann. Nucl. Energy*, 112:354 – 363, 2018.

B. Montagnini and V. Pierpaoli. The time-dependent rectilinear transport equation. *Transport Theory and Statistical Physics*, 1:59–75, 1971.

A. Mylonakis, H. Yi, P. Vinai, and C. Demazière. Neutron noise simulations in a heterogeneous system: A comparison between a diffusion-based and a discrete ordinates solver. In *Proceedings of M&C2019*, Portland USA, 2019.

N. Olmo-Juan, C. Demazière, T. Barrachina, R. Miró, and G. Verdú. PARCS vs CORE SIM neutron noise simulations. *Progress in Nuclear Energy*, 115:169 – 180, 2019.

I. Pazsit. Investigation of the space-dependent noise induced by a vibrating absorber. *Atomkernenergie*, 30:29–35, 1977.

I. Pazsit. The linearization of vibration-induced noise. *Ann. Nucl. Energy*, 11:441–454, 1984.

I. Pazsit and G. T. Analytis. Theoretical investigation of the neutron noise diagnostics of two-dimensional control rod vibrations in a PWR. *Ann. Nucl. Energy*, 7:171–183, 1980.

I. Pazsit and C. Demazière. Noise techniques in nuclear systems. In D. Cacuci, editor, *Handbook of nuclear engineering*, chapter 14, pages 1629–1737. Springer Verlag, 2010.

I. Pazsit and V. Dykin. The role of the eigenvalue separation in reactor dynamics and neutron noise theory. *J. Nucl. Sci. Technol.*, 55:484–495, 2018.

I. Pazsit and J. Karlsson. On the perturbative calculation of the vibration noise by strong absorber. *Ann. Nucl. Energy*, 24:449–466, 1996.

F. Rahnema. Boundary condition perturbations in transport theory. *Nucl. Sci. Eng.*, 124:320–326, 1996.

U. Rohde, M. Seidl, S. Kliem, and Y. Bilodid. Neutron noise observations in German KWU built PWRs and analyses with the reactor dynamics code DYN3D. *Annals of Nuclear Energy*, 112: 715 – 734, 2018.

A. Rouchon. *Analyse et développement d'outils numériques déterministes et stochastiques résolvant les équations du bruit neutronique et applications aux réacteurs thermiques et rapides*. PhD thesis, Université Paris-Saclay, 2016.

A. Rouchon and R. Sanchez. Analysis of Vibration-induced Neutron Noise Using One-dimension Noise Diffusion Theory. In *Proceedings of ICAPP2015*, Nice, France, 2015.

A. Rouchon, A. Zoia, and R. Sanchez. A new Monte Carlo method for neutron noise calculations in the frequency domain. *Ann. Nucl. Energy*, 102:465–475, 2017.

A. Rouchon, W. Jarrah, and A. Zoia. The new neutron noise solver of the Monte Carlo code TRIPOLI-4. In *Proceedings of M&C2019*, Portland USA, 2019.

R. Sanchez. Some comments in neutron noise theory. *Ann. Nucl. Energy*, 86:88–98, 2015.

J. A. Thie. *Power Reactor Noise*. American Nuclear Society, 1981.

A. Vidal-Ferrándiz, A. Carreno, D. Ginestar, C. Demazière, and G. Verdú. A time and frequency domain analysis of the effect of vibrating fuel assemblies on the neutron noise. *Ann. Nucl. Energy*, 137:107076, 2020.

A. M. Weinberg and H. C. Schweinler. Theory of oscillating absorber in a chain reactor. *Phys. Rev.*, 74:851–863, 1948.

M. M. R. Williams. Reactivity changes due to the random vibration of control rods and fuel elements. *Nuclear Science and Engineering*, 39:144–150, 1970.

M. M. R. Williams. *Random Processes in Nuclear Reactors*. Pergamon Press, Oxford, 1974.

G. Wing. *An introduction to transport theory*. Wiley and sons, New York, 1962.

T. Yamamoto. Monte Carlo method with complex-valued weights for frequency domain analyses

of neutron noise. *Ann. Nucl. Energy*, 58:72–79, 2013.

T. Yamamoto. Implementation of a frequency-domain neutron noise analysis method in a production-level continuous energy Monte Carlo code: verification and application to a BWR. *Ann. Nucl. Energy*, 115:494–501, 2018.

T. Yamamoto and H. Sakamoto. Decomposition of neutron noise in a reactor into higher-order mode components and investigation of the space and frequency dependence. *Progr. Nucl. Energy*, 117:103098, 2019.

H. Yi, P. Vinai, and C. Demazière. Discrete ordinates solver with diffusion synthetic acceleration for simulations of 2-d and 2-energy group neutron noise problems. In *Proceedings of M&C2019*, Portland USA, 2019.